Discontinuous Jump Behavior of the Energy Conversion in Wind Energy Systems

Pyei Phyo Lin,[1,*] Matthias Wächter,[1] M. Reza Rahimi Tabar,[2,1] and Joachim Peinke[1]

[1] *ForWind, Institute of Physics, University of Oldenburg, Oldenburg, Germany*

[2] *Department of Physics, Sharif University of Technology, Tehran 11155-9161, Iran*

(Received 13 January 2023; revised 27 June 2023; accepted 11 July 2023; published 16 August 2023)

The power conversion process of a wind turbine can be characterized by a stochastic differential equation (SDE) of the power output conditioned to certain fixed wind speeds. An analogous approach can also be applied to the mechanical loads on a wind turbine, such as generator torque. The constructed SDE consists of the deterministic and stochastic terms, the latter corresponding to the highly fluctuating behavior of the wind turbine (power output of a wind turbine or wind speed). Here we show how advanced stochastic analysis of the noise contribution can be used to show different operating modes of the conversion process of a wind turbine. The parameters of the SDE, known as Kramers-Moyal coefficients, are estimated directly from the measurement data. Clear evidence is found that both continuous diffusion noise and discontinuous jump noise are present. The difference in the noise contributions indicates different operational regions. In particular, we observe that the jump character or discontinuity in power production has a significant contribution in the regions where the control system switches strategies. We find that there is a high increase in jump amplitude near the transition to the rated region, and the switching strategies cannot result in a smooth transition. The proposed analysis provides new insights into the control strategies of the wind turbine.

DOI: 10.1103/PRXEnergy.2.033009

I. INTRODUCTION

Wind energy is considered one of the most promising solutions in the global shift from fossil fuels to clean and sustainable energy sources. According to a report by Windeurope [1], Europe is projected to install approximately 105 GW of new wind energy capacity between 2021 and 2025. However, the unpredictable and intermittent nature of wind poses challenges for accurately predicting wind energy production, which is crucial for ensuring a stable energy supply [2–5]. Moreover, this variability in wind conditions can lead to premature mechanical fatigue failure [6,7]. It is recognized that the current industry standard defined by the International Electrotechnical Commission (IEC61400) does not adequately capture the variability in wind and wind power [7,8]. In particular, when examining time series of a wind turbine's power output, rapid fluctuations can occur, exceeding 50% of the rated power [9]. These short-term power fluctuations in the megawatt range impose additional stress on the turbine's drive train and the power grid, as they may accumulate within a wind farm rather than being averaged out [8,9].

In this contribution, our focus is on providing a statistically advanced characterization of the power fluctuations observed in wind turbines. Recent research has demonstrated that the power conversion process of a wind turbine can be effectively modeled using a stochastic Langevin differential equation, which describes the power output P conditioned to specific wind speeds u within small intervals [9–11]. Similar modeling approaches have also been applied to analyze the mechanical loads on wind turbines, such as the generator torque T [12]. The key advantage of this approach lies in its ability to directly extract the model equations, in the form of Langevin equations, from the available data. Consequently, this model captures the stochastic, turbulent, and intermittent nature of wind power [9,13–15]. While previous efforts in Langevin modeling of wind turbine conversion dynamics have primarily focused on the deterministic component of the power time series, the question of how to accurately account for the abrupt, large power fluctuations mentioned earlier has remained unanswered.

The Langevin equation provides a description of a diffusion process characterized by a continuous trajectory. It comprises two main components: a deterministic term and a continuous stochastic term, which can be modeled using a Wiener process (Brownian motion). The estimation

*pyei.phyo.lin@uol.de

of the model's parameters, namely the drift and diffusion coefficients, can be directly obtained from the available measurement data [16–18]. These parameters are commonly referred to as Kramers-Moyal (KM) coefficients and are typically considered up to second order in the Langevin equation. In the case of the continuous process, higher-order coefficients are considered negligible and theoretically approach zero.

Looking at the high-temporal resolution wind power data, one can observe segments of the time series that resemble a diffusive process [see Fig. 1(a)]. However, there are also periods characterized by sudden and significant jumps in the delivered power, as depicted in Fig. 1(b).

Here, our objective is to investigate the extent to which these jumps necessitate an extension of the stochastic description. If the higher-order KM coefficients (≥ 3) are proved to be significant, they would indicate noncontinuity in the process [18,19]. One possible approach to model this behavior is to extend the Langevin diffusion process to a jump-diffusion process. This entails introducing an additional discontinuous stochastic term to account for the jump process, which we assume can be modeled by a Poisson process. With this more comprehensive stochastic framework, two additional parameters emerge: the jump rate and the jump amplitude. We demonstrate how these parameters can be estimated from the higher-order KM coefficients. The purpose of this analysis is to provide a more realistic stochastic characterization of the power output of a wind turbine. The implications for control strategies and the potential for improved modeling of wind energy resources in power grids will also be discussed in this paper.

Our aim is to provide a procedure for estimating the general stochastic jump-diffusion process with Wiener and Poisson noise, enabling a more detailed analysis of the wind power conversion dynamics in a wind turbine using an advanced stochastic characterization and modeling. In this study, we analyze the data obtained from a wind turbine at a resolution of 1 Hz [20]. The paper is structured as follows. Firstly, we describe the analyzed data, providing relevant details. Then, we summarize the stochastic analysis method, illustrating how the contributions of diffusion and jump fluctuations can be quantified and separated. Lastly, we present the results of the data analysis for power output conditioned to wind speed. Additionally, we investigate the stochastic relationship between generator torque and generator rotational speed.

II. STOCHASTIC DATA ANALYSIS OF THE WIND ENERGY SYSTEM

A. Data description

The measurement data used in this study are obtained from wind turbines located within an onshore wind farm. The wind farm occupies an area of approximately 4 km^2 and consists of 12 identical variable-speed, pitch-regulated

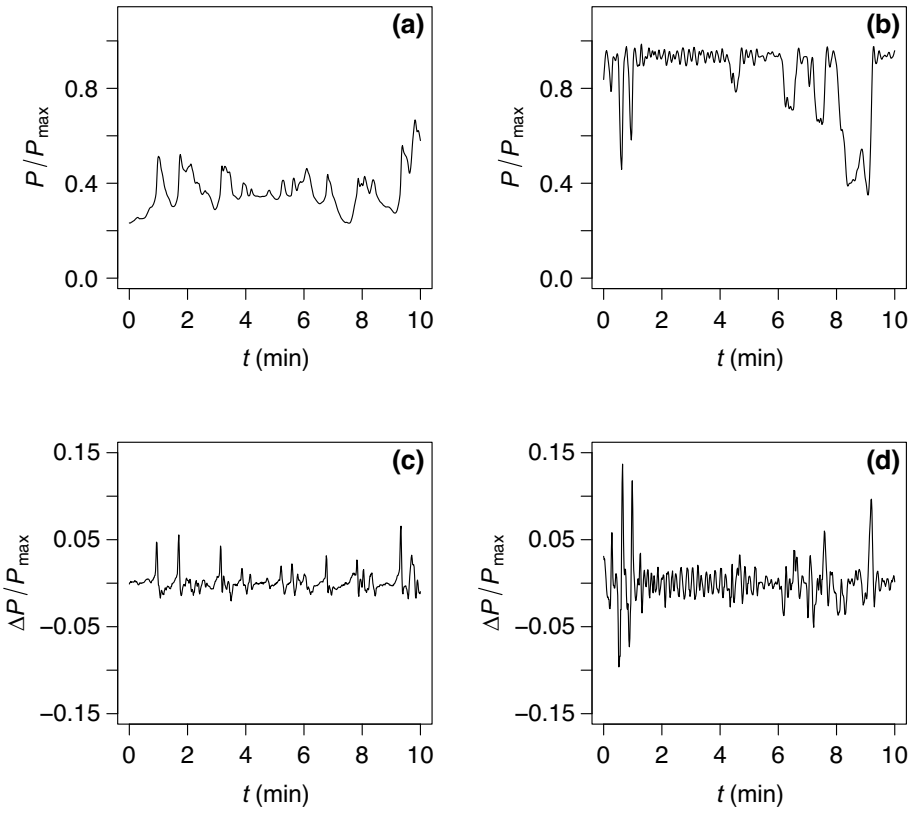

FIG. 1. Wind power time series, spanning the period of ten minutes. Panel (a) shows the period where the power changes are not very large. Panel (b) shows the period where the power changes are very large, up to about 40% of the rated power. Increments $\Delta P := P(t + \Delta t) - P(t)$ emphasize the fluctuations and are shown for sampling period $\Delta t = 1$ s in (c) and (d).

wind turbines. Each turbine has a rated power of around 2 MW [20]. All the data used in our analysis have been normalized relative to their respective maximum values.

The measured quantities include the net electrical power output, denoted as P, generated by the wind turbine, the wind speed u measured on the nacelle using a cup anemometer, and the rotational speed measured in revolutions per minute, denoted as Ω, of the generator. The torque T on the generator is calculated based on the power and the rotational speed using the appropriate relationship,

$$T = \frac{60\,\mathrm{s}}{2\pi}\frac{P}{\Omega}. \tag{1}$$

All measurements were performed at a sampling frequency $f_s = 1$ Hz. The measurement campaign was conducted over a period of eight months, from June 2009 till February 2010. A subset of the data is available online [21], which has already been published in Ref. [4].

B. Power conversion process described by stochastic dynamics

Assuming the validity of a diffusive process, the power conversion process of a wind turbine can be modeled by a stochastic Langevin equation describing the power output P conditioned on a fixed wind speed u [9–11]:

$$dP(t,u) = D^{(1)}(P|u)\,dt + \sqrt{D^{(2)}(P|u)}\,dW_t, \tag{2}$$

Here, W_t represents a Wiener process, which is a scalar Brownian motion. The functions $D^{(1)}(P|u)$ and $D^{(2)}(P|u)$ are the drift and diffusion coefficients, respectively, and in the context of the Langevin equation (2), they correspond to the first- and second-order KM coefficients. These KM coefficients, denoted as $K^{(j)}(P|u)$, can be directly determined from the available data of power output P for each wind speed u. The estimation of these coefficients involves the calculation of conditional incremental averages (cf. Refs. [16,18]) as

$$K^{(j)}(P|u) = \lim_{\Delta t\to 0}\frac{M^{(j)}(P|u;\Delta t)}{\Delta t}, \tag{3}$$

where

$$M^{(j)}(P|u;\Delta t) = \langle (P(t+\Delta t) - P(t))^j\,|_{P(t)=P,\,u(t)=u}\rangle. \tag{4}$$

The Langevin equation describes a continuous diffusion process where $K^{(j)}(P|u) = 0$ for $j \geq 3$ and $D^{(j)}(P|u) = K^{(j)}(P|u)$ for $j = 1, 2$. Further details on methods of this estimation [22] can be found in Refs. [16,17] and in Appendix D. The modeling of a time series using the Langevin equation [Eq. (2)] requires the satisfaction of a necessary condition involving the fourth- and second-order conditional moments. Specifically, for small Δt, the condition is given by [23]

$$\Theta(P|u;\Delta t) = 3\frac{(M^{(2)}(P|u;\Delta t))^2}{M^{(4)}(P|u;\Delta t)} \simeq 1 \tag{5}$$

We demonstrate that the wind power data do not satisfy this condition, indicating that the present variability in the wind power data cannot be captured by the Langevin equation.

All the higher-order KM coefficients vanish when the fourth-order KM coefficient $K^{(4)}(P|u)$ is negligible according to the Pawula theorem [24,25].

When a stochastic process exhibits sharp changes or discontinuities at certain instants, higher-order Kramers-Moyal coefficients, particularly $K^{(4)}(P|u)$, become not negligible. In such cases, an extension of the Langevin-type modeling is necessary, incorporating an additional jump noise [18,19,26–29].

Such a jump-diffusion dynamics for a power conversion process is given by

$$dP(t,u) = D^{(1)}(P|u)\,dt + \sqrt{D^{(2)}(P|u)}\,dW_t + \xi\,dJ_t, \tag{6}$$

where again W_t is a Wiener process, $D^{(1)}(P|u)$ and $D^{(2)}(P|u)$ are the drift and diffusion coefficients. In the following, we make the assumption that J_t is a Poisson jump process. This assumption will be further validated and confirmed below. Coefficient ξ is the jump size, which is assumed to be normally distributed, $\xi \sim N(0,\sigma_\xi^2)$, with zero mean and variance σ_ξ^2. Variance σ_ξ^2 is also known as the jump amplitude. Here J_t is a Poisson jump process that is a zero-one jump process with jump rate $\lambda(P|u)$ [18,30]. The drift and diffusion coefficients and the jump rate are now related to the KM coefficients $K^{(j)}(P|u)$ in the following way [18,19]:

$$D_j^{(1)}(P|u) = K^{(1)}(P|u), \tag{7}$$

$$D_j^{(2)}(P|u) + \lambda(P|u)\langle\xi^2\rangle = K^{(2)}(P|u), \tag{8}$$

$$\lambda(P|u)\langle\xi^j\rangle = K^{(j)}(P|u) \quad \text{for } j > 2. \tag{9}$$

Since ξ has a zero mean, its second-order moment is given by $\langle\xi^2\rangle = \sigma_\xi^2$, which serves as the definition of the jump amplitude. From Eq. (7), we can observe that the estimation of the drift coefficient applies to both the diffusion process described by the Langevin equation and the jump-diffusion process. In the following analysis, we further explore the noise component by relaxing the assumption of $K^{(4)}(P|u) = 0$. This allows us to gain a more comprehensive understanding of the system dynamics and the influence of higher-order Kramers-Moyal coefficients.

The jump amplitude, denoted as σ_ξ^2, and the jump rate λ, can be estimated using Eq. (9) with $j = 4$ and 6, along

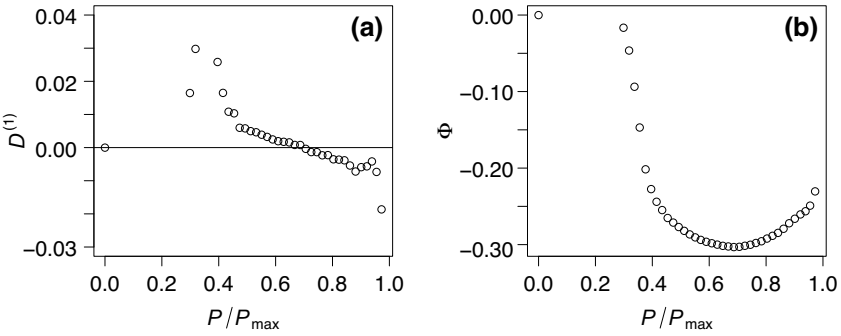

FIG. 2. Drift coefficient $D^{(1)}(P|u)$, (a), and corresponding potential Φ, (b), for the wind speed of $u = 0.41u_{max}$. Zero crossings of the drift coefficient $D^{(1)}(P|u) = 0$ or local minima of the drift potential Φ are stable fixed points that describe the equilibrium dynamics.

with Wick's theorem [31,32] for Gaussian random variables. The expressions for the jump amplitude and jump rate are given by

$$\sigma_\xi^2(P|u) = \frac{K^{(6)}(P|u)}{5K^{(4)}(P|u)} \tag{10}$$

and

$$\lambda(P|u) = \frac{K^{(4)}(P|u)}{3\sigma_\xi^4(P|u)}, \tag{11}$$

respectively. These equations provide estimates of the jump amplitude and jump rate based on the values of the corresponding Kramers-Moyal coefficients.

C. Results

1. Results for the electrical power output

a. Drift coefficients. To investigate the relationship between wind speed and power, we analyze the Kramers-Moyal coefficients $K^{(j)}(P|u)$ for specific wind speed ranges. We choose fixed wind speed values within a bin size of approximately $0.02u_{max}$ and assume stationarity within each wind speed bin. The stationarity of each subset is confirmed using the augmented Dickey-Fuller (ADF) test [33–35]. For example, we consider the power time series conditioned on the wind speed bin $0.4u_{max} < u < 0.42u_{max}$. The ADF test is performed, and the test statistic yields $DF = -22.69$, which is less than the critical value $DF_{crit} = -3.43$. Additionally, the p-value is found to be $p < 0.01$, indicating a rejection of the null hypothesis and confirming the stationarity of the subset.

In the first step, we determine the drift coefficients. The zero crossings of the drift coefficient, $D^{(1)}(P|u) = 0$, provide intuition into the stable and unstable fixed points or equilibria within each wind speed bin. If the slope of $D^{(1)}$ is negative, the zero crossings represent stable fixed points, whereas zero crossings with positive slope indicate unstable fixed points [10,36]. Alternatively, this can be interpreted in terms of a drift potential, denoted as Φ, which is defined as $\Phi = -\int_P D^{(1)}(P|u)\,dP$. The zero crossings with negative slope in the drift correspond to minima of the drift potential. Fixed points are calculated by linear interpolation between two points left and right of the zero crossings with negative slopes. Errors are estimated by linear interpolation of the upper and lower bounds on the standard

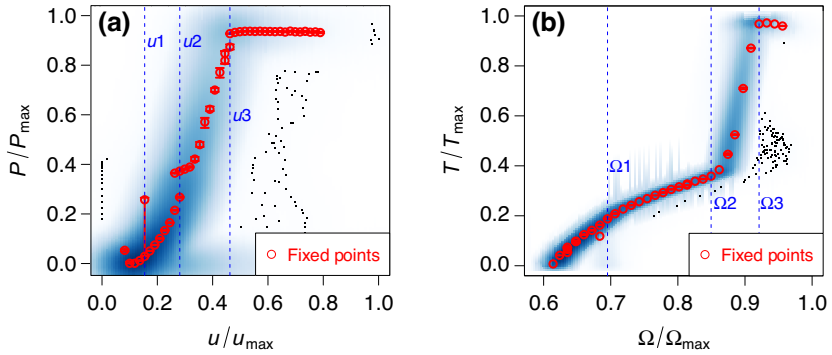

FIG. 3. Characteristic power curve, (a), determined from the zero crossings of the drift coefficients at each wind speed bin and characteristic torque curve, (b), at each rotational speed bin, presented in red open circles. They are also called the Langevin power curve (LPC) and Langevin torque curve (LTC), respectively. The blue background shows the density scatter plot of the measurement data and darker regions indicate that more data points are available. The black dots are the outliers of the density scatter plot. Three distinct states (u1, u2, and u3) for LPC and (Ω1, Ω2, and Ω3) for LTC that separate the operational regions are marked by blue dashed lines.

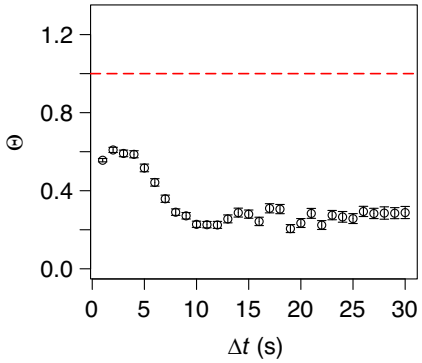

FIG. 4. Checking the relation Θ in Eq. (5) at the rated power for different time lags Δt, which are not equal to unity (red dashed line). This rules out that the wind rated power fluctuations are diffusive.

errors of the drift coefficients at these two points. Figure 2 illustrates an example of a drift coefficient and its corresponding potential for a wind speed of $u = 0.41u_{\max}$. This direct approach enables the detection of fixed points based on the properties of the drift coefficient.

For each wind speed bin, there can exist one or multiple stable fixed points. These fixed points allow us to reconstruct the characteristic power curve, known as the Langevin power curve (LPC) [37,38]. Figure 3(a) illustrates the LPC, where the stable fixed points are plotted. These fixed points enable us to define different operational states of the wind turbine. In our analysis, we identify three distinct states, u1, which is near the cut-in wind speed where the wind turbine starts operating, u2, at which the possible control switching is observed from the characteristic curve, and u3, which is near the transition to the rated power, which separate the operational regions, indicated by blue dashed lines in Fig. 3(a). It is important to note that near the operation point u2, we observe the discontinuous shifting of fixed points. Such details cannot be captured by the standard averaging procedure used to define the power curve, as defined by IEC61400 [39]. These findings highlight the need for a more advanced and comprehensive approach to characterize the operational behavior of the wind turbine.

The analysis and characterization of the power output of a wind turbine using the Langevin equation (2) or the diffusion process have been extensively studied in Refs. [10,11,20]. These studies primarily focused on the drift coefficient and did not consider the higher-order KM coefficients. In contrast, our work here places emphasis on the noisy component and specifically evaluates the higher-order KM coefficients. By incorporating these higher-order coefficients, we aim to provide a more comprehensive understanding of the stochastic behavior and variability in the power output of a wind turbine.

b. Stochastic behaviour. To characterize the stochastic variability of the power time series, we initially examined Eq. (5) to determine whether the Langevin equation is capable of describing the observed variability or not. To this end, our analysis shows that the wind power fluctuations do not satisfy the prerequisite for being classified as diffusion processes, which in turn can be modeled using the Langevin equation, as proved in Ref. [23]; the results are provided in Fig. 4. Hence, in order to capture the nondiffusive behaviors observed in the data, we need to employ a model that can effectively account for these characteristics.

In our analysis, we focus on estimating the functions and parameters in the jump-diffusion processes, which extend the Langevin dynamics when higher-order KM coefficients ($j \geq 3$) are nonzero. To validate the assumption of a Poisson process associated with J_t, we examine the waiting times in the rated power time series. We select a threshold level, such as 0.8, and identify the waiting times τ between consecutive exceedances of this threshold.

In Fig. 5, we plot the probability density function (PDF) of the waiting times. Notably, this distribution is well fitted by an exponential distribution, $p(\tau) = \lambda e^{-\lambda\tau}$ with $\lambda = 0.04$, providing evidence for the validity of our assumption regarding the Poisson process associated with J_t. However, the values of the Poisson jump rate λ depend on different conditioning or binning of the wind speed u as well as the power P. The details and further assumptions are discussed next.

As explained in Sec. II B, we can investigate the jump amplitude and jump rate using the KM coefficients $K^{(4)}(P|u)$ and $K^{(6)}(P|u)$. In our analysis, we simplify the process by assuming constant parameters σ_ξ^2 and λ for the

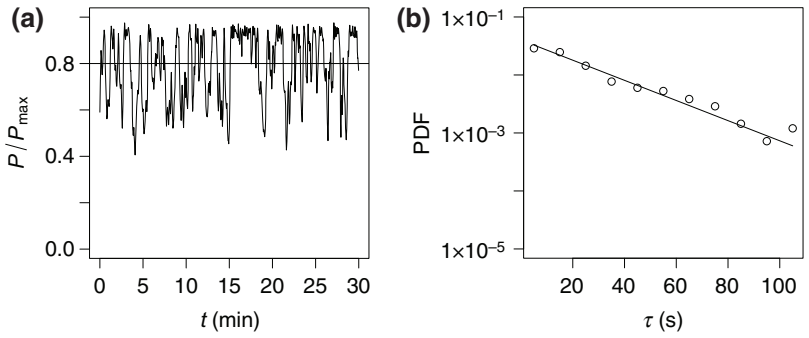

FIG. 5. Power time series is shown in (a). The level $P/P_{\max} = 0.8$ has been chosen to estimate τ for waiting times between two jumps in rated power. The probability density function (PDF) of waiting times τ is well fitted with an exponential distribution $p(\tau) = \lambda e^{-\lambda\tau}$, where $\lambda \simeq 0.04$ s^{-1}, on a semilogarithmic scale, (b).

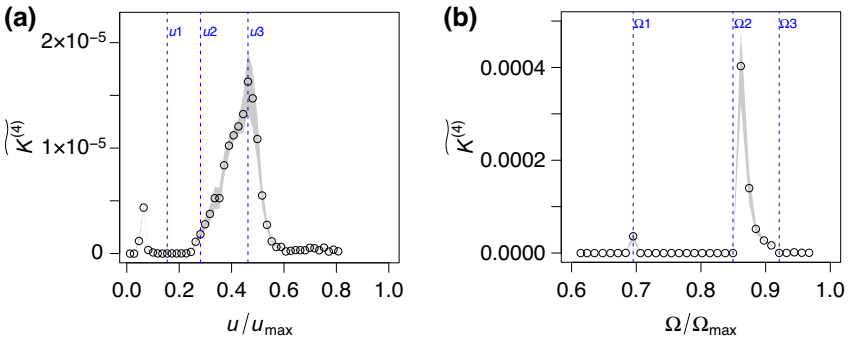

FIG. 6. The median of the fourth-order KM coefficient, $\widetilde{K^{(4)}}$, over the power bins for each wind speed bin (a) and over the torque bins for each rotational speed bin (b). There is an increase of $\widetilde{K^{(4)}}$ near the transition to the rated region. Statistical uncertainties are shown as a gray-shaded background. Blue dashed lines are the distinct states observed from the fixed point analysis; see Fig. 3.

jump process and $D^{(2)}$ for the diffusion process. Although the P dependence of these parameters can be studied, we keep the discussion simpler here.

In Figs. 11(a), 11(d) and 11(g) in Appendix A, we provide some examples of diffusion coefficient $D^{(2)}(P|u)$ for the wind speed $u = (0.25, 0.4, 0.5)u_{\max}$, along with their medians represented by solid black lines. It is worth noting that we can obtain more accurate results near the fixed point due to better data coverage. However, in regions with less data (farther away from the fixed point), the results become noisier and outliers may be observed. To mitigate the impact of extreme outliers on averaged values, we report medians as the constant parameters instead of means [40]. Statistical uncertainties are also estimated using the median absolute deviation. Additional examples as well as the calculation of uncertainties are provided in Appendix A.

In Fig. 6(a), we observe an increase in $\widetilde{K^{(4)}}(u)$ near state u3, which corresponds to the transition point to the rated power. This behavior indicates the presence of nondiffusive noise. Consequently, we proceed to analyze the higher-order KM coefficients to determine the jump amplitude $\widetilde{\sigma_\xi^2}(u)$ and jump rate $\widetilde{\lambda}(u)$ for each wind speed, as depicted in Figs. 7(a) and 7(c). The jump amplitude $\widetilde{\sigma_\xi^2}$ is found to be highest between states u2 and u3, just below the transition to the rated power region where the switching of the control strategy plays a major role. On the other hand, the jump rate $\widetilde{\lambda}$ is highest in the region of rated power.

In order to quantify the overall jump contribution, we determine the product $\widetilde{\lambda\sigma_\xi^2}$ as shown in Fig. 8(c). The figure shows that the jump contribution $\widetilde{\lambda\sigma_\xi^2}$ is highest around state u3, indicating that jumps play a significant role in that region. This suggests that nondiffusive behaviors, captured by the jump-diffusion model, are important in describing the power variability. Additionally, the diffusion-to-jump ratio $\widetilde{D^{(2)}/\lambda\sigma_\xi^2}$ in Fig. 8(e) provides insights into whether

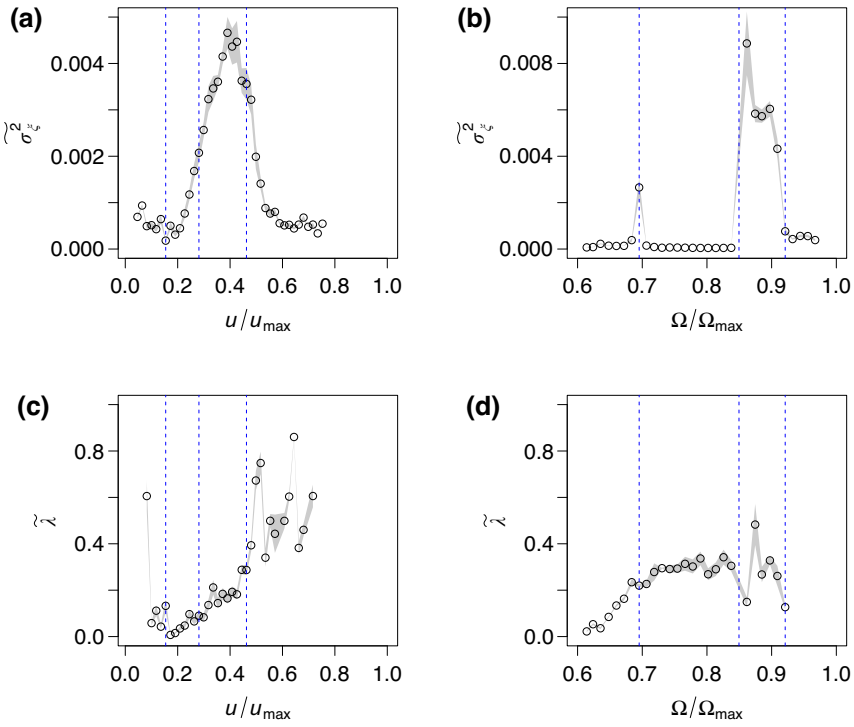

FIG. 7. The median of jump amplitude, $\widetilde{\sigma_\xi^2}$, over the power bins for each wind speed bin (a) and over the torque bins for each rotational speed bin (b). There is a significant increase in the jump amplitude near the transition to the rated region. The median of the jump rate, $\widetilde{\lambda}$, over the power bins for each wind speed bin (c) and over the torque bins for each rotational speed bin (d). Again, we find a significant increase in the jump rate after the transition to the rated region and a small increase near the cut-in region for power analysis. The jump rate for torque analysis is similar in between all three distinct states shown by blue dashed lines, as in Fig. 3. Statistical uncertainties are shown as a gray-shaded background.

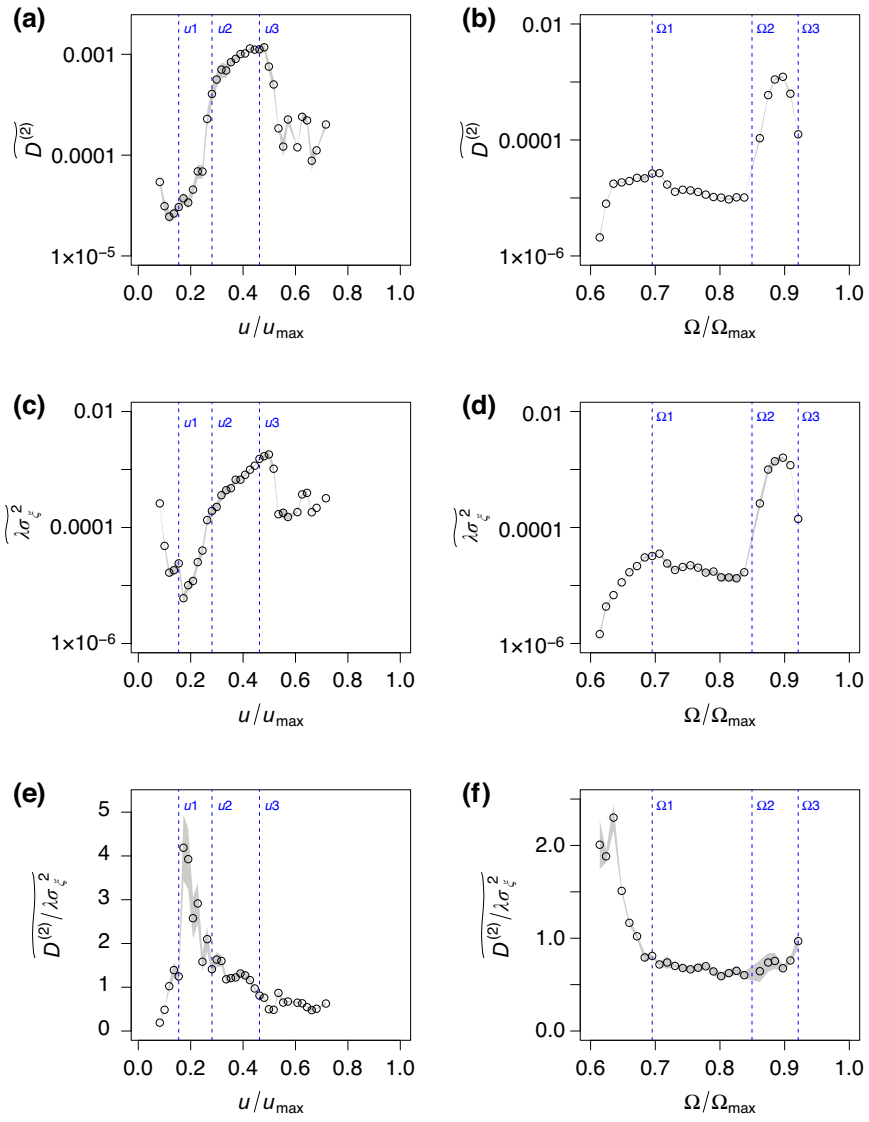

FIG. 8. The median of diffusion coefficient, $\widetilde{D^{(2)}}$, (a), overall jump contribution, $\widetilde{\lambda\sigma_\xi^2}$, (c), and the diffusion-to-jump ratio, $\widetilde{D^{(2)}/\lambda\sigma_\xi^2}$, (e), over the power bins for each wind speed bin, and respective quantities over the torque bins for each rotational speed bin in (b), (d) and (f). Subfigures (a)–(d) are plotted in semilogarithmic scale for better visualization. Statistical uncertainties are shown as a gray-shaded background. Blue dashed lines are the distinct states observed from fixed point analysis; see Fig. 3.

diffusive or jump noise dominates. A large ratio indicates more diffusive noise dominance, while a small ratio indicates more jump noise dominance. From the plot, we can see that jump noise is dominant in the rated power region after state u3, while diffusive noise is dominant between states u1 and u2, coinciding with the lowest jump contribution $\lambda\sigma_\xi^2$ in Fig. 8(c). This analysis helps us understand the relative importance of diffusive and jump components in the power variability.

To check how our results are robust to finite-order time Δt, we use the Itô-Taylor expansion, introduced in Refs. [18,27], which is a straightforward way to reduce the error of estimations of KM coefficients with finite time step (see Appendix D). We find a few percent of derivations in estimations of KM coefficients with increasing order of approximation from first to third order; see also Ref. [41] for finite-order time corrections. We also find evidence that our data are Markovian down to the sampling interval employing a least-squares method [18,42].

The analysis conducted in this subsection highlights two notable findings. First, it confirms the presence of a jump process in the power variability, indicating the need to incorporate this component in an advanced stochastic model. The jump process captures the sudden changes and discontinuities observed in the wind turbine behavior. Second, the analysis reveals that well below the rated power, the power variability is primarily driven by diffusive stochastic behavior. However, as the wind turbine approaches the transition to the rated power region, the contribution of jump noise becomes increasingly important. This indicates that the jumpy nature of the power fluctuations plays a significant role in the behavior of the wind turbine near its operational limits.

In order to validate the ansatz of the jump-diffusion process, we reconstruct time series from the jump-diffusion stochastic equation [Eq. (6)]. To assess the statistical similarity between the reconstructed and empirical time series, we examine the PDFs of power increments at different

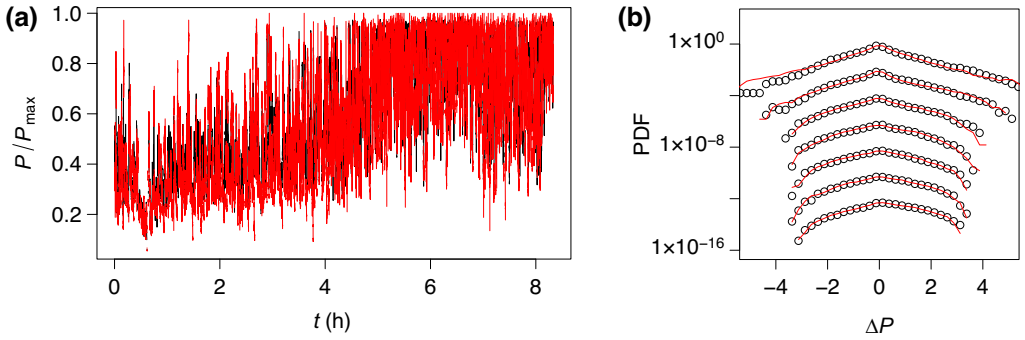

FIG. 9. Time series of empirical wind power data (black) and reconstructed data with the jump-diffusion process (a), and their normalized increment statistics (PDFs), i.e., $\Delta P(\Delta t) = (P(t+\Delta t) - P(t))/\mathbf{sd}(P(t+\Delta t) - P(t))$, (b), for different lags, $\Delta t = (1, 10, 30, 60, 600, 1800, 3600)$ s (from top to bottom). **sd** stands for standard deviation. The PDFs are shifted along the vertical axis for convenience of presentation.

time lags Δt. We note that the variance of these PDFs corresponds to the autocorrelation or power spectrum, while the shape of the PDFs enables the study of higher-order two-point statistics. Our analysis demonstrates that the simulated time series accurately reproduces the tails of the PDFs with high precision. The results are shown in Fig. 9.

2. Results for the generator torque

Apart from the dynamical dependence of power on the wind speed, another central characteristic of the wind turbine is the generator torque T versus the rotational speed Ω [12]. The generator torque was calculated from power and rotational speed data according to Eq. (1), whereas the rotational speed was measured independently. A similar stochastic approach like for the power and wind speed is applied to the torque and rotational speed dynamics $T(t, \Omega)$, next. Based on the drift coefficient, a characteristic curve like the Langevin power curve is calculated, as shown in Fig. 3(b). We refer to it as the Langevin torque curve (LTC). We again mark three distinct states ($\Omega 1$, $\Omega 2$, and $\Omega 3$) with blue dashed lines that can be inferred from the fixed point analysis of the rotational speed described in Appendix B. These states coincide with the fixed points or the minimal potentials of the rotational speed that the control system prefers to approach.

Next, we also determine the jump contribution $\lambda\sigma_\xi^2$ and the diffusion-to-jump ratio $D^{(2)}/\lambda\sigma_\xi^2$ for each rotational speed bin; see Figs. 8(d) and 8(f). In Fig. 8(d), we see that the median of the jump contribution $\widetilde{\lambda\sigma_\xi^2}$ becomes dominant in the region between $\Omega 2$ and $\Omega 3$ [cf. Fig. 3(b)] at relatively high rotational speed values. Outside this regime, jump noise does not dominantly contribute to the dynamics. On the other hand, the median of the diffusion-to-jump ratio $\widetilde{D^{(2)}/\lambda\sigma_\xi^2}$ takes its largest values at low values of rotational speed. At the rotational speeds below state $\Omega 1$, diffusive behavior is dominant; see Fig. 8(f).

The conclusions from the previous subsection II C 1 also apply to the torque analysis in an analogous way. Similar to the power characteristic, a jump process is also present for the torque characteristic, which could be expected as we compute the torque from power and rotational speed. Diffusive stochastic behavior is dominating for low rotational speed ($\Omega < \Omega 1$), but in the region $\Omega > \Omega 1$, diffusive and jumpy behavior seem to be more balanced for the torque case; see Fig. 8(f).

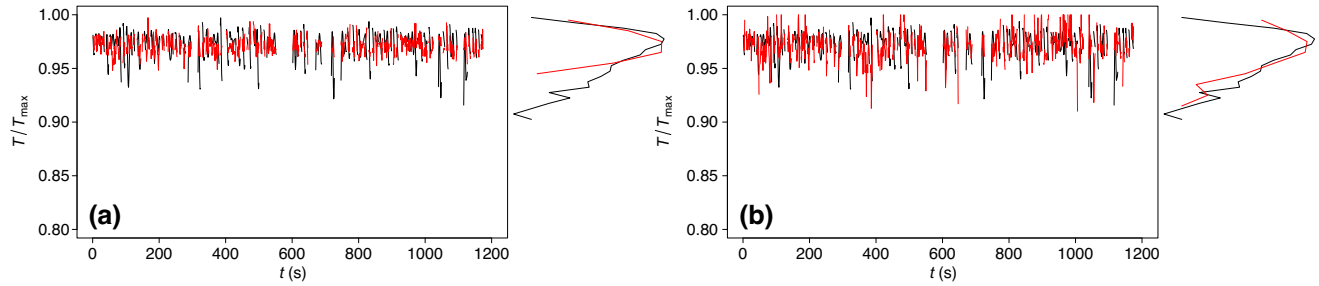

FIG. 10. Reconstruction of the rated torque with the diffusion process (a) and jump-diffusion process (b). The PDFs of the reconstructed time series on a semilogarithmic scale are shown on the right sides. For the reconstruction, we use the following parameters: $D^{(1)}(T) = -0.47T/T_{\max} + 0.45$, $D^{(2)} = 4.6 \times 10^{-5}\ \mathrm{s}^{-1}$, $\lambda = 0.2\ \mathrm{s}^{-1}$, and $\sigma_\xi^2 = 4.5 \times 10^{-4}$. We can clearly see that the jump-diffusion process better fits the empirical data than the pure diffusion process.

Additionally, we also simulated the rated torque with both diffusion and jump-diffusion processes and compared it with the empirical data, as shown in Fig. 10, together with the corresponding PDFs on the right in order to validate our ansatz of the jump-diffusion model. Here we can clearly see that the jump-diffusion process better fits the empirical data than the pure diffusion process.

III. CONCLUSION AND OUTLOOK

In our work, we investigate the contribution of the higher-order KM coefficients to the stochastic dynamics of the power conversion process of a wind turbine. As described in Sec. II B, these higher-order coefficients allow us to quantify the contributions of diffusive behavior and jump noise, and indicate that discontinuities in the trajectory of the measurement data are due to the stochastic jump noise. The main results are that we can quantify with our proposed method how the amplitudes and the ratio of the two noise contributions change in different operating ranges of a wind turbine. The region below rated power seems to provide the highest values of the amplitudes ($D^{(2)}$ and σ_ξ^2). Sometimes the maximal values are found for the transition states defined by the fixed point characteristics. The ratio between the contributions of the diffusive and jumpy noise shows that at low wind speed and low power a diffusive noise is dominating, whereas for higher power, more jump noise is present, with some detailed differences for power and torque. All this indicates that it is the interplay between the stochastic driving wind speed and the reacting control system that determines the noise contribution.

In particular, the jump contribution is closely linked to the control system, especially in the regime of rated power or torque. To our interpretation, we can observe the rapid changes of σ_ξ^2 in Fig. 7(b). Interestingly, this is more prominent in the torque signal than in the power signal. It is well known that the control system is not operating directly with the wind signal but with toque T and the rotational speed Ω.

Near states $\Omega 1$, $\Omega 2$, and $\Omega 3$ there are three distinct operational rotational speeds Ω that the control system prefers to approach. It is a common control strategy to avoid certain resonance frequencies of the structure in order to mitigate excessive loads. We show this by evaluating the drift potential $\Phi(\Omega)$ of the rotational speed. The minima of this potential correspond to the preferred rotational speeds; see Appendix B. Moreover, looking at Fig. 3(b), between states $\Omega 2$ and $\Omega 3$, there is a steep gradient that enforces a large change in generator torque T at only a small regime in rotational speed Ω. In this range, we also observe that there is a huge increase in both diffusive and jump noise by more than 2 orders of magnitude; see Figs. 8(b) and 8(d). As a remark, we also applied our analysis to the data of other similar turbines in the wind farm and it gave similar results, as shown in Appendix C.

So far, we have used the stochastic methods to characterize the dynamics of the wind energy conversion process. It goes without saying that the characterization can be used to compare different turbines quantitatively. Potential failures in the control system should be detectable by comparison of the different stochastic terms. One may see how some noise contributions change with time as the system gets old, or one may show how different wind turbines or different control strategies perform differently in a dynamic sense. Together with detailed knowledge of a specific turbine, this should also be useful for monitoring, e.g., performance or structural health. The presented successful characterization of the dynamics of a wind turbine driven by noisy inflow indicates that such a stochastic approach may also be promising for other machines operating under unsteady conditions. With our procedure, it seems to be possible to quantify an effective dynamics that also includes eventual smart control systems.

Apart from jump-diffusion modeling of power and torque stochastic dynamics, there is interest in modeling them using a Lévy-driven Langevin process. These models are particularly suitable for processes that have infinite Kramers-Moyal coefficients for $j \geq 2$, provided they have finite drift coefficient ($j = 1$) [43]. For the analyzed data, we find finite values for all Kramers-Moyal coefficients.

Finally, we would like to point out that besides this characterization the stochastic methods presented here also deliver the explicit form of the stochastic differential equations. Thus, it is also possible to use our results as very efficient dynamics models for power and torque. Long time simulations can be done easily. Such models are of interest for the simulation of the contribution of wind energy to the power grid and for the simulation of loads.

ACKNOWLEDGMENTS

The authors would like to thank Vlaho Petrović and Christian Philipp for helpful discussions. We acknowledge financial support by the Federal Ministry for Economic Affairs and Climate Action of Germany in the framework of the projects "WEA-Doktor" (reference 0324263A) and "WiSAbigdata" (reference 03EE3016A).

APPENDIX A: MEDIAN AS A ROBUST ESTIMATOR

Statistically, we can obtain more accurate results near the fixed point due to the better coverage of data, whereas for regions with less data (farther away from the fixed point), the results become more noisy and outliers are seen. A robust method to estimate the typical values of $D^{(2)}(P|u)$, $\lambda(P|u)\sigma_\xi^2(P|u)$, and $D^{(2)}(P|u)/[\lambda(P|u)\sigma_\xi^2(P|u)]$, as examples, is to use the

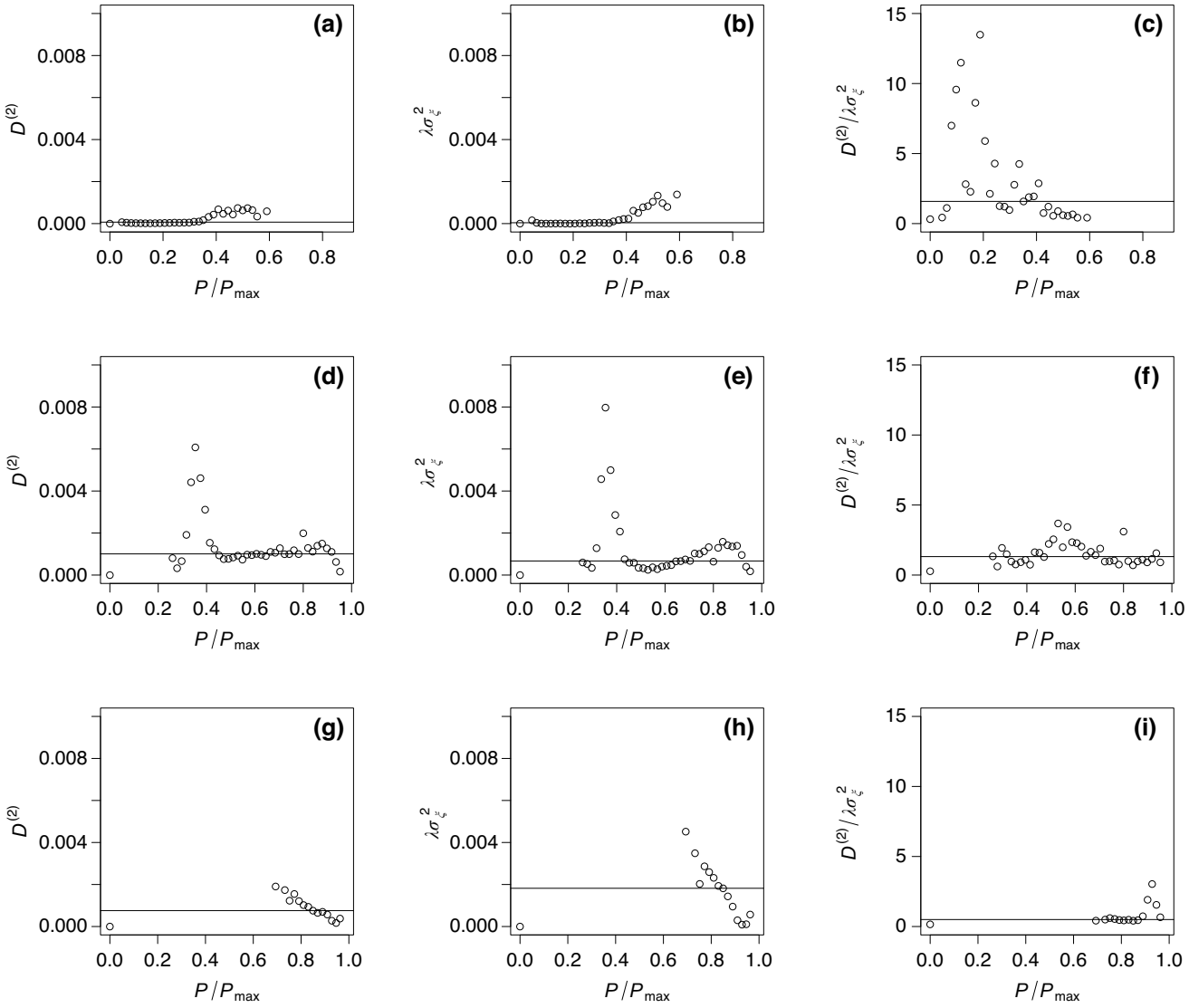

FIG. 11. Diffusion coefficient $D^{(2)}(P|u)$, jump parameter $\lambda(P|u)\sigma_\xi^2(P|u)$, and diffusion-to-jump ratio $D^{(2)}(P|u)/[\lambda(P|u)\sigma_\xi^2(P|u)]$ for wind speeds of $u = 0.25u_{\max}$ (a)–(c), $u = 0.4u_{\max}$ (d)–(f), and $u = 0.5u_{\max}$ (g)–(i). The solid black lines are their respective medians $\widetilde{D^{(2)}}(u)$, $\widetilde{\lambda\sigma_\xi^2}(u)$, and $\widetilde{D^{(2)}/\lambda\sigma_\xi^2}(u)$. The fixed point for this wind speed bin is $P = (0.16, 0.62, 0.94)P_{\max}$. Statistically, more accurate results can usually be obtained near the fixed point due to the better coverage of data. By using the median, our results are more robust to outliers far away from the fixed points.

medians $\widetilde{D^{(2)}}(u)$, $\widetilde{\lambda\sigma_\xi^2}(u)$, and $\widetilde{D^{(2)}/\lambda\sigma_\xi^2}(u)$ to mitigate the impact of extreme outliers on averaged values, as shown by the solid lines in Fig. 11.

The uncertainties are determined by the median absolute deviations (MADs). We write the median of a variable $\mathbf{X}$ as $\widetilde{\mathbf{X}}$ and the MAD as $\widetilde{|X_i - \widetilde{\mathbf{X}}|}$.

APPENDIX B: DRIFT POTENTIAL OF THE ROTATIONAL SPEED

We analyzed all the data of rotational speed Ω in the range of $0.6\Omega_{\max}$ and $\Omega_{\max}$ without any conditioning or binning on other variables. We evaluated the drift coefficient $D^{(1)}(\Omega)$ and then determined the drift potential, $\Phi(\Omega) = -\int_\Omega D^{(1)}(\Omega)\, d\Omega$, which is plotted in Fig. 12. Minima of the drift potential correspond to the stable fixed points or equilibria. Here we can observe three minima that define the three states $\Omega 1$, $\Omega 2$, and $\Omega 3$ that the control system prefers to approach. It is a common control strategy to avoid certain resonance frequencies of the structure in order to mitigate excessive loads, as shown in Fig. 3.

In Fig. 12(b), we can clearly observe a minimum around state $\Omega 1$. From our results in Figs. 6, 7, and 8, there is also a slight increase in noises around this state. This indicates that the control system of the wind turbine starts switching

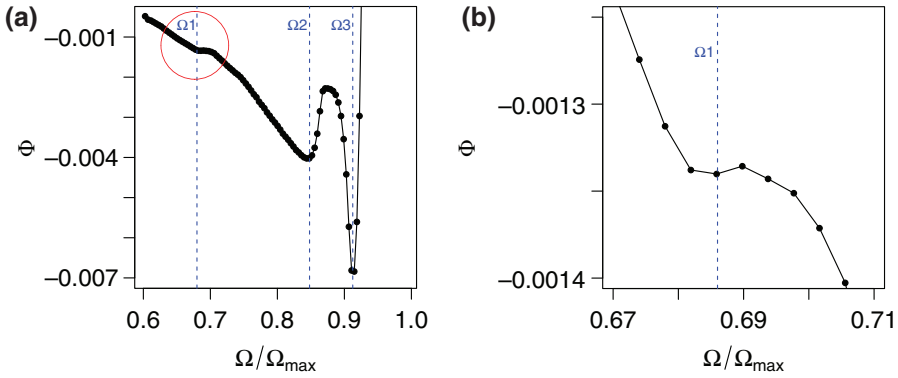

FIG. 12. (a) Drift potential $\Phi(\Omega)$ determined in the range of $0.6\Omega_{\max}$ and $\Omega_{\max}$. Minima of the drift potential correspond to the stable fixed points or equilibria. Here we can observe three minima that define the three states Ω1, Ω2, and Ω3, as shown in Fig. 3. The minimum around state Ω1, which is presented with the red circle, is enlarged in (b).

the strategies at this state around Ω1. As a remark, we only calculated the deterministic potential that reflects the mechanical and control mechanism of the wind turbine.

APPENDIX C: RESULTS ON THE ANALYSIS OF ANOTHER TURBINE IN THE WIND FARM

In the main sections of the paper, we analyzed the data of turbine number 6 in the wind farm that consists of 12 turbines. The analysis of the other turbines also gives similar results. Results of analysing the data of turbine number 7 are shown here as another example in Fig. 13, which is similar to Figs. 3 and 8 in the main text.

APPENDIX D: ESTIMATION OF KM COEFFICIENTS AND FINITE-ORDER CORRECTION OF CONDITIONAL MOMENTS

We consider a projection of the two-dimensional (P, u) state space to one dimension (P) by choosing a binning

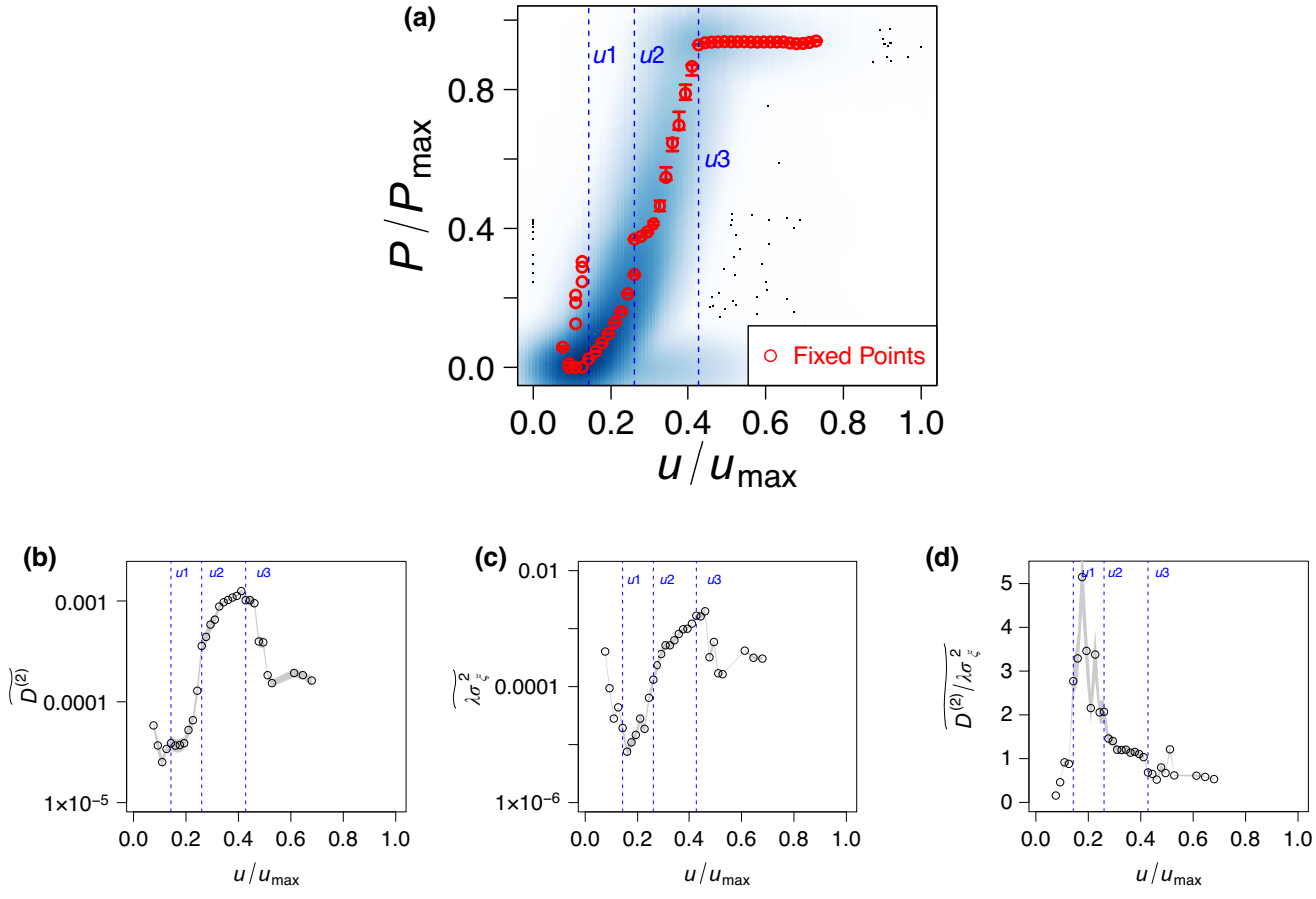

FIG. 13. Characteristic power curve (a), diffusion coefficient (b), jump parameter (c), and diffusion-to-jump ratio (d), analyzed with different turbine in the same wind farm.

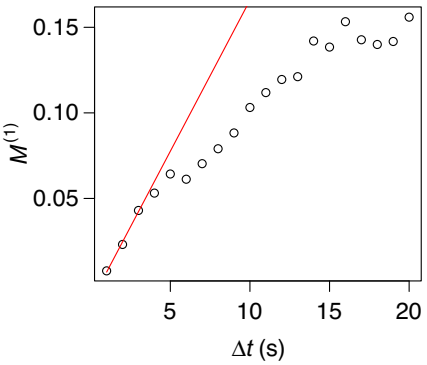

FIG. 14. Estimation of the KM coefficient from the conditional moment. In this example, for $u \simeq 0.38u_{\max}$ and $P \simeq 0.43P_{\max}$, the first-order conditional moments are estimated for different time lags $\Delta t = (1, 2, 3, \ldots)$ s and a linear regression is performed for the first three time lags. The slope of the linear regression is the KM coefficient.

for the wind speed u. In each segment of the time series, with finite width of the wind speed bin, the power can have fluctuations and this is the reason why we are reporting the KM coefficients of power in each segment with respect to the mean of the wind speed bin.

In practice, for each u and P bin, the conditional moments are estimated for different time lags $\Delta t = (1, 2, 3, \ldots)$ s and a linear regression is performed for the first three time lags, as shown in Fig. 14. The slope of the linear regression is the KM coefficient. Actually, the KM coefficient is the limit $\lim_{\Delta t \to 0}[M^k(P|u, \Delta t)/\Delta t]$.

To check how robust our results are to finite-order time Δt, we used an Itô-Taylor expansion introduced by Stanton [27], which is an easier way to reduce the error of estimations of KM coefficients with finite time steps. We find a few percent of deviations in the estimations of KM coefficients with increasing order of approximation from first to third order (see also Ref. [18]).

For the wind power conditioned on wind speed, the first-order approximation for Kramers-Moyal conditional moments is given by

$$M^{(j)}(P|u, \Delta t) = \langle (P(t + \Delta t) - P(t))^j |_{P(t)=P, u(t)=u} \rangle + \mathcal{O}(\Delta t)^2, \tag{D1}$$

the second-order approximation is given by

$$M^{(j)}(P|u, \Delta t) = \tfrac{1}{2}[4\langle (P(t + \Delta t) - P(t))^j |_{P(t)=P, u(t)=u} \rangle - \langle (P(t + 2\Delta t) - P(t))^j |_{P(t)=P, u(t)=u} \rangle] + \mathcal{O}(\Delta t)^3, \tag{D2}$$

the third-order approximation is given by

$$M^{(j)}(P|u, \Delta t) = \tfrac{1}{6}[18\langle (P(t + \Delta t) - P(t))^j |_{P(t)=P} \rangle - 9\langle (P(t + 2\Delta t) - P(t))^j |_{P(t)=P, u(t)=u} \rangle + 2\langle (P(t + 3\Delta t) - P(t))^j |_{P(t)=P, u(t)=u} \rangle] + \mathcal{O}(\Delta t)^4, \tag{D3}$$

etc., as shown in Ref. [27]. Equations (D1)–(D3) allow us to estimate the KM conditional moments and therefore the KM coefficients with different precision.

[1] WindEurope, Wind energy in europe: 2020 statistics and the outlook for 2021-2025, https://windeurope.org/intelligence-platform/product/wind-energy-in-europe-2020-statistics-and-the-outlook-for-2021-2025/ (2021).

[2] J.-F. Muzy, R. Baïle, and P. Poggi, Intermittency of surface-layer wind velocity series in the mesoscale range, Phys. Rev. E **81**, 056308 (2010).

[3] R. Calif and F. G. Schmitt, Multiscaling and joint multiscaling description of the atmospheric wind speed and the aggregate power output from a wind farm, Nonlinear Process. Geophys. **21**, 379 (2014).

[4] M. Anvari, G. Lohmann, M. Wächter, P. Milan, E. Lorenz, D. Heinemann, M. R. R. Tabar, and J. Peinke, Short term fluctuations of wind and solar power systems, New J. Phys. **18**, 063027 (2016).

[5] K. Schmietendorf, J. Peinke, and O. Kamps, The impact of turbulent renewable energy production on power grid stability and quality, Eur. Phys. J. B **90**, 222 (2017).

[6] T. Mücke, D. Kleinhans, and J. Peinke, Atmospheric turbulence and its influence on the alternating loads on wind turbines, Wind Energy **14**, 301 (2011).

[7] M. Wächter, H. Heißelmann, M. Hölling, A. Morales, P. Milan, T. Mücke, J. Peinke, N. Reinke, and P. Rinn, The turbulent nature of the atmospheric boundary layer and its impact on the wind energy conversion process, J. Turbul. **13**, N26 (2012).

[8] H. Haehne, J. Schottler, M. Waechter, J. Peinke, and O. Kamps, The footprint of atmospheric turbulence in power grid frequency measurements, Europhys. Lett. **121**, 30001 (2018).

[9] P. Milan, M. Wächter, and J. Peinke, Turbulent Character of Wind Energy, Phys. Rev. Lett. **110**, 138701 (2013).

[10] E. Anahua, S. Barth, and J. Peinke, Markovian power curves for wind turbines, Wind Energy **11**, 219 (2008).

[11] J. Gottschall and J. Peinke, How to improve the estimation of power curves for wind turbines, Environ. Res. Lett. **3**, 015005 (2008).

[12] P. G. Lind, I. Herráez, M. Wächter, and J. Peinke, Fatigue load estimation through a simple stochastic model, Energies **7**, 8279 (2014).

[13] O. Kamps, in *Wind Energy - Impact of Turbulence*, edited by M. Hölling, J. Peinke, and S. Ivanell (Springer Berlin Heidelberg, Berlin, Heidelberg, 2014), p. 67.

[14] H. Liu, Y. Jin, N. Tobin, and L. P. Chamorro, Towards uncovering the structure of power fluctuations of wind farms, Phys. Rev. E **96**, 063117 (2017).

[15] T. Braun, M. Waechter, J. Peinke, and T. Guhr, Correlated power time series of individual wind turbines: A data driven model approach, J. Renew. Sustain. Energy **12**, 023301 (2020).

[16] R. Friedrich, J. Peinke, M. Sahimi, and M. Reza Rahimi Tabar, Approaching complexity by stochastic methods: from biological systems to turbulence, Phys. Rep. **506**, 87 (2011).

[17] P. Rinn, P. G. Lind, M. Wächter, and J. Peinke, The Langevin approach: An R package for modeling Markov processes, J. Open Res. Softw. **4**, e34 (2016).

[18] M. R. R. Tabar, *Analysis and Data-Based Reconstruction of Complex Nonlinear Dynamical Systems: Using the Methods of Stochastic Processes* (Springer, Cham-Switzerland, 2019).

[19] M. Anvari, M. Rahimi Tabar, J. Peinke, and K. Lehnertz, Disentangling the stochastic behaviour of complex time series, Nat. Sci. Rep. **6**, 35435 (2016).

[20] P. Milan, M. Wächter, and J. Peinke, Stochastic modeling and performance monitoring of wind farm power production, J. Renew. Sustain. Energy **6**, 033119 (2014).

[21] Data can be downloaded under http://uni-oldenburg.de/fileadmin/user_upload/physik/ag/twist/Forschung/Daten/AnvariEtAl2016_ExampleData_WindPowerAndIrradianceData.zip.

[22] KM coefficients of a Langevin process in $x(t)$ are defined for $j = 1, 2$ as $K^{(j)}(x,t) = D^{(j)}(x,t) = (1/j!) \lim_{\Delta t \to 0} \langle (x(t+\Delta t) - x(t))^j |_{x(t)=x} \rangle / \Delta t$ in Refs. [16,17]. The code to determine the KM coefficients is available as an R package in Ref. [17]. In order to stay consistent with the jump-diffusion process, our definition differs by a factor of $1/j!$, and $dW_t = \int_t^{t+dt} \Gamma(s)\, ds$, where $\langle \Gamma(t) \rangle = 0$ and $\langle \Gamma(t)\Gamma(t') \rangle = \delta(t-t')$. The corresponding Fokker-Planck equation will be $\partial p(x,t)/\partial t = -\partial [D^{(1)}(x,t) p(x,t)]/\partial x + \frac{1}{2}\partial^2 [D^{(2)}(x,t)\, p(x,t)]/\partial x^2$.

[23] K. Lehnertz, L. Zabawa, and R. Tabar, Characterizing abrupt transitions in stochastic dynamics, New J. Phys. **20**, 113043 (2018).

[24] R. F. Pawula, Approximation of the linear Boltzmann equation by the Fokker-Planck equation, Phys. Rev. **162**, 186 (1967).

[25] H. Risken and T. Frank, *The Fokker-Planck Equation: Methods of Solution and Applications*, Springer Series in Synergetics (Springer Berlin Heidelberg, Berlin, Heidelberg, 1996).

[26] P. Tankov, *Financial Modelling with Jump Processes*, Chapman and Hall/CRC Financial Mathematics Series (CRC Press, New York, 2003).

[27] R. Stanton, A nonparametric model of term structure dynamics and the market price of interest rate risk, J. Finance **52**, 1973 (1997).

[28] M. Johannes, The statistical and economic role of jumps in continuous-time interest rate models, J. Finance **59**, 227 (2004).

[29] F. M. Bandi and T. H. Nguyen, On the functional estimation of jump-diffusion models, J. Econom. **116**, 293 (2003).

[30] F. Hanson, *Applied Stochastic Processes and Control for Jump Diffusions: Modeling, Analysis, and Computation*, Advances in Design and Control (Society for Industrial and Applied Mathematics, Philadelphia, 2007).

[31] L. Isserlis, On certain probable errors and correlation coefficients of multiple frequency distributions with skew regression, Biometrika **11**, 185 (1916).

[32] G. C. Wick, The evaluation of the collision matrix, Phys. Rev. **80**, 268 (1950).

[33] D. A. Dickey and W. A. Fuller, Distribution of the estimators for autoregressive time series with a unit root, J. Am. Stat. Assoc. **74**, 427 (1979).

[34] D. A. Dickey and W. A. Fuller, Likelihood ratio statistics for autoregressive time series with a unit root, Econometrica **49**, 1057 (1981).

[35] W. Fuller, *Introduction to Statistical Time Series*, Wiley Series in Probability and Statistics (Wiley, Hoboken, New Jersey, 2009).

[36] J. Gottschall and J. Peinke, Stochastic modelling of a wind turbine's power output with special respect to turbulent dynamics, J. Phys.: Conf. Ser. **75**, 012045 (2007).

[37] P. Milan, T. Mücke, A. Morales, M. Wächter, and J. Peinke, in *Proceedings of EWEC 2010* (WindEurope, Warsaw, 2010).

[38] M. Wächter, P. Milan, T. Mücke, and J. Peinke, Power performance of wind energy converters characterized as stochastic process: Applications of the Langevin power curve, Wind Energy **14**, 711 (2011).

[39] IEC, *Wind energy generation systems - Part 1: Design requirements. IEC 61400-1:2019 International Standard, 2019.*, Tech. Rep. (IEC, 2019).

[40] P. Huber and E. Ronchetti, *Robust Statistics*, Wiley Series in Probability and Statistics (Wiley, Hoboken, New Jersey, 2011).

[41] L. Rydin Gorjão, D. Witthaut, and P. G. Lind, jumpdiff: A Python library for statistical inference of jump-diffusion processes in observational or experimental data sets, J. Stat. Softw. **105**, 1 (2023).

[42] F. Ghasemi, J. Peinke, M. Sahimi, and M. R. Rahimi Tabar, Regeneration of stochastic processes: An inverse method, Eur. Phys. J. B **47**, 411 (2005).

[43] S. Siegert and R. Friedrich, Modeling of nonlinear Lévy processes by data analysis, Phys. Rev. E **64**, 041107 (2001).